IJMAO

International Journal of Mathematical Analysis and Optimization: Theory and Applications
Vol. 2020, No. 1, pp. 764 - 779

Dynamic Analysis of a Debonding Piezoelectric Sensor Layer of a Smart Beam

Isede, H. A.[1*], Taiwo, T. J.[2]

1*, Department of Mathematics, University of Lagos, Lagos, Nigeria.
2, Department of Mathematics, University of Benin, Benin City, Nigeria.
*Corresponding author: hisede@unilag.edu.ng

Article Info
Received: 04 April 2020 Revised: 21 June 2020
Accepted: 08 July 2020 Available online: 01 September 2020

Abstract

In this paper, a specific study of the dynamic analysis of a debonding piezoelectric sensor/actuator layer attached to a host beam in a smart structure using finite element method was carried out. The results were obtained by using the Euler-Bernoulli beam theory to derive the governing equations converted to systems of matrix equations by the Galerkin finite element method, and solved numerically by Maple 18 package. It was observed that increases in the bending stiffness and the density of the composite beam decreases the displacement of the transverse displacement of the piezoelectric sensor/actuator layer, while increases in the axial stiffness and density of the composite beam increases the flexural (axial) displacement of the piezoelectric sensor/actuator layer and thereby impacting the debonding length of the attached piezoelectric patch, with respect to time.

Keywords And Phrases: Debonding; Piezoelectric Actuator/Sensor; Finite Element Analysis; Axial displacement; Transverse displacement.
MSC2010: 74H15, 74S05,74k10.

1 Introduction

Certain materials produce electric charges on their surfaces as a consequence of applying mechanical stress. The induced charges are proportional to the mechanical stress. This is called the direct piezoelectric effect and was discovered in quartz by Piere and Jacques Curie in 1880. Materials showing this phenomenon also conversely have geometric strain proportional to an applied electric field. This is the converse piezoelectric effect. The word "piezo" means "pressure"; hence the original meaning of the word piezoelectricity is "pressure- electricity." Piezoelectricity is extensively utilized in the fabrication of various devices such as transducers, actuators, surface acoustic wave devices, frequency control and so on [1, 2]. Piezoelectric materials are classified into: single-crystal materials, piezoceramics, piezopolymers, piezocomposites and piezofilms. Each of these

IJMAO

International Journal of Mathematical Analysis and Optimization: Theory and Applications
Vol. 2020, No. 1, pp. 764 - 779

piezoelectric materials is used as piezoelectric actuators/sensors which have become key components in electroresistive devices such as precision positioners, miniature ultrasonic motor and adaptive mechanical dampers. They practically work in three categories as, positioners, motors and vibration suppressors, Sohrabi and Muliana [3]. Examples of piezoelectric actuators are zirconatetitanate [PZT, Pb(Zr,Ti)O3], barium stannatetitanate system [Ba(Sn,Ti)O3], Lezgy-Nazargah et al. [4]. Piezoelectric actuators/sensors are designed as multilayer, bimorph and moonie, Seely and Chattopadhyay [5]. Two of the most popular actuator designs are the multilayers and bimorphs. The multilayer, in which roughly 100 thin piezoelectric/electrostrictive ceramic sheets are stacked toegther, has the advantages of low driving voltage (100V), quick response (10 μs), high generative force (100 N), and high electromechnical coupling. But the displacment, on the order of 10 μm, is not sufficient for some applications, Shijie [6]. This contrasts with the characterisitcs of the bimorph which consists of multiple piezoelectric and elastic plates bonded together to generate a large bending displacement of several hundred μm, but has relatively low response time (1 ms) and generative force (1N), Neto et al. [7]. Debonded piezoelectric actuator layer is a layer that is not perfectly bonded to the host structure by the adhesive layer; often as a result of mechanical vibrations. When this occurs in smart structures, it affects the dynamics of the structure. In Sun et al. [8], a detailed study of the effect of debonding had been considered on the dynamics of piezoelectric actautors/sensors attached to a host beam in a smart structures with significant results. Boundary Element (BE) analyses performed on delaminated composite structures repaired by active piezoelectric patches are presented by Alaimo et al. [9],where they investigated the effect of the frictional contact condition on the fracture mechanics behavior of actively repaired delaminated composite structures. The study of Sun et al. [8] specifically investigated the debonding effects on the host beam layer of the composite beam. Our objective in the present study is to investigate the effects of debonding on the axial and transverse displacement of the piezoelectric actuator layer.

2 Formulation of the Problem

The dynamics responses of the piezoelectric actuator layer were determined using the finite element method that begins with discretizing the piezoelectric actuator layer into elements. The finite element model was then developed using linear Lagrange interpolation function and Hermite cubic interpolation function respectively for the axial and transverse governing equations. Both the elemental and assembled stiffness, mass and load vector were then derived. The systems of assembled matrix equations were then solved computationally after applying the boundary conditions. The diagram below shows the structural set up of the host beam with bonded piezoelectrics. The piezoelectrics are shown bonded to the host beam by adhesive on top and below. The orientation is such that the axial axis is the x-axis while the transverse axis is the z-axis [10].

IJMAO

International Journal of Mathematical Analysis and Optimization: Theory and Applications
Vol. 2020, No. 1, pp. 764 - 779

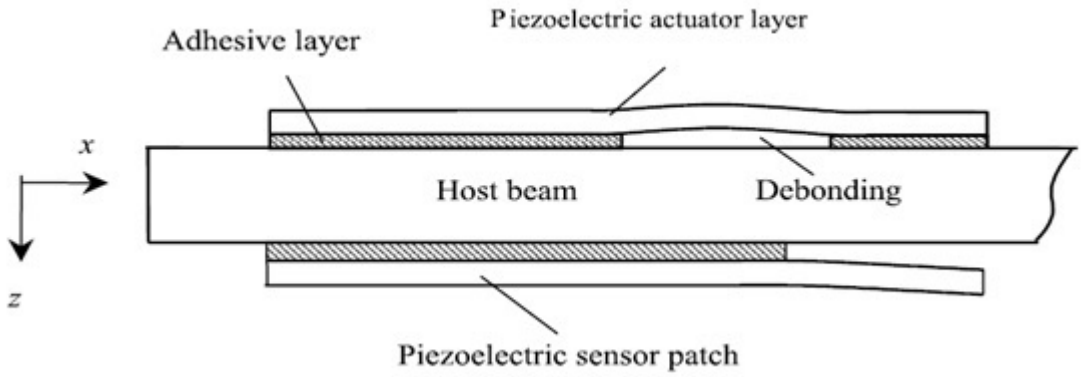

Figure 1: The beam and piezoelectric layers with debonding [8].

In deriving the governing equation, we assumed that there is no stress transferring between the host beam and piezoelectric actuator layer through the adhesive layer. And contact and friction between the debonded surfaces are not considered for simplicity. From the above diagram, it can be seen that the composite beam can be divided into segments, the segments containing only the host beam, and the segments including the host beam bonded with two piezoelectric patches on its upper and lower surfaces. So, the free body diagram of the piezoelectric actuator layer, adhesive layer and host beam were shown in Fig. 2.

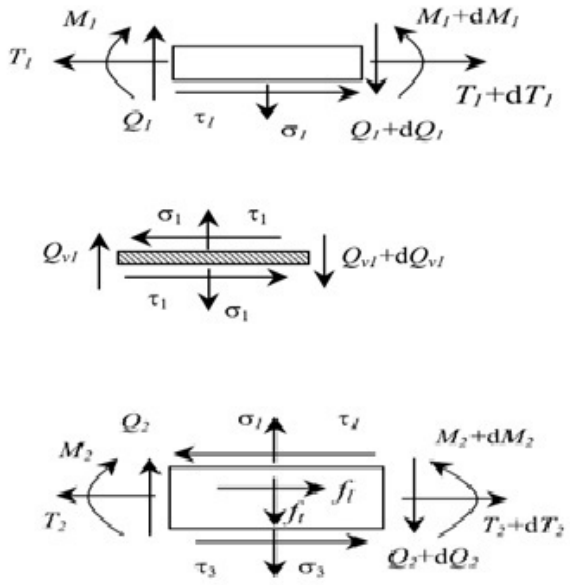

Figure 2: Free body diagram of the piezoelectric, the adhesive and the host beam [8].

Now we derive the governing equations for axial and transverse displacement of the the piezoelectric

IJMAO

International Journal of Mathematical Analysis and Optimization: Theory and Applications
Vol. 2020, No. 1, pp. 764 - 779

actuator layer, by using the Euler-Bernoulli beam theory in line with work of D. Sun et al. [8]. From fig. 2, the following equations of motion were obtained for the actuator layer and host beam using the momentum principle:

$$\rho_1 A_1 \frac{\partial^2 u_1}{\partial t^2} = \frac{\partial T_1}{\partial x} + b\tau, \tag{2.1}$$

$$\rho_1 A_1 \frac{\partial^2 w_1}{\partial t^2} = \frac{\partial Q_1}{\partial x} + b\sigma, \tag{2.2}$$

$$\frac{\partial M_1}{\partial x} + \frac{bh_1}{2}\tau - Q_1 = 0, \tag{2.3}$$

$$\rho_2 A_2 \frac{\partial^2 u_2}{\partial t^2} = \frac{\partial T_2}{\partial x} - b\tau + f_l(x,t), \tag{2.4}$$

$$\rho_2 A_2 \frac{\partial^2 w_2}{\partial t^2} = \frac{\partial Q_2}{\partial x} - b\sigma + f_t(x,t), \tag{2.5}$$

$$\frac{\partial M_2}{\partial x} + \frac{bh_2}{2}\tau - Q_2 = 0. \tag{2.6}$$

From figure 2 and equations (2.1 to 2.6) the subscripts 1 and 2 represent the sensor layer and the host beam respectively; where u is the longitudinal displacement in mid plane, w is the transverse displacement, h denotes the thickness, b is the width of the composite beam, τ and σ are the shear and peel stress of the adhesive layer, T, Q and M are the axial force, transverse shear force and bending moment respectively, $f_l(x,t)$ and $f_t(x,t)$ are the axial and transverse loads per unit length on the host beam. The equivalent mass densities per unit length of the sensor and the host beam are

$$\rho_1 A_1 = \rho_1 b h_1 + \frac{\rho_{ad} b h_{ad}}{2}, \tag{2.7}$$

$$\rho_2 A_2 = \rho_2 b h_2 + \frac{\rho_{ad} b h_{ad}}{2}, \tag{2.8}$$

respectively, with half of the mass of the adhesive layer added. The axial stress resultant and the bending moment for the actuator layer can be written respectively as:

$$T_1 = G\frac{\partial u_1}{\partial x} - b e_{31} V, \tag{2.9}$$

$$M_1 = -D\frac{\partial^2 w_1}{\partial x^2} - b e_{31} r_1 V, \tag{2.10}$$

where r_1 is the z-coordinate value of the mid plane of the actuator layer from its neutral plane and V is the voltage applied on the actuator along its thickness direction, e_{31} is the piezoelectric stress constant of the actuator layer. G and D are the axial and bending stiffness respectively.
Using the constant shear and peel strain assumption [4] the shear and peel stress in the adhesive layer are given by:

$$\tau = k_b \frac{Y_{ad}}{2(1+v_{ad})h_{ad}}\gamma, \tag{2.11}$$

$$\sigma = \frac{k_b Y_{ad}(1-V_{ad})}{(1-2v_{ad})(1+v_{ad})h_{ad}}(W_2 - W_1). \tag{2.12}$$

Where k_b is a parameter characterizing the bonding conditions and h_{ad} is the thickness of the adhesive layer, Y_{ad} and V_{ad} are the Young's modulus and Poisson's ratio of the adhesive layer respectively, and γ is the shear strain which takes the form:

$$\gamma = \frac{1}{2}\left(\frac{\partial w_1}{\partial x} + \frac{\partial w_2}{\partial x}\right) + \frac{1}{2h_{ad}}\left(h_1\frac{\partial w_1}{\partial x} + h_2\frac{\partial w_2}{\partial x}\right) + \frac{u_2 - u_1}{h_{ad}}. \tag{2.13}$$

IJMAO

International Journal of Mathematical Analysis and Optimization: Theory and Applications
Vol. 2020, No. 1, pp. 764 - 779

From equation (2.3),

$$Q_1 = \frac{\partial M_1}{\partial x} + \frac{bh_1}{2}\tau.$$

Substituting equations (2.7), (2.9 - 2.12) into (2.1) and (2) yield

$$\rho_1 A_1 \frac{\partial^2 u_1}{\partial t^2} - G\frac{\partial^2 u_1}{\partial x^2} - \frac{bk_b P_{ad}}{2}\left[\frac{\partial w_1}{\partial x} + \frac{\partial w_2}{\partial x} + \frac{1}{h_{ad}}\left(h_1\frac{\partial w_1}{\partial x} + h_2\frac{\partial w_2}{\partial x}\right) + 2\frac{u_2 - u_1}{h_{ad}}\right] = -be_{31}\frac{\partial V}{\partial x}, \tag{2.14}$$

$$\rho_1 A_1 \frac{\partial^2 w_1}{\partial t^2} + D\frac{\partial^4 w_1}{\partial x^4} - \frac{h_a bk_b P_{ad}}{4}\left[\frac{\partial^2 w_1}{\partial x^2} + \frac{\partial^2 w_2}{\partial x^2} + \frac{1}{h_{ad}}\left(h_1\frac{\partial^2 w_1}{\partial x^2} + h_2\frac{\partial^2 w_2}{\partial x^2}\right) + \frac{2}{h_{ad}}\left(\frac{\partial u_2}{\partial x} - \frac{\partial u_1}{\partial x}\right)\right] - \frac{k_b Y_{ad} b}{h_{ad}}(w_2 - w_1) = -be_{31}r_1\frac{\partial^2 V}{\partial x^2}. \tag{2.15}$$

In the present study $k_b = 0$, for the debonded part. The equation of motion with the surviving subscript 1 removed becomes, for the sensor layer only:

$$-\frac{\partial}{\partial x}\left(G\frac{\partial u}{\partial x}\right) + \rho A\frac{\partial^2 u}{\partial t^2} + q_1 = 0, \tag{2.16}$$

$$\frac{\partial^2}{\partial x^2}\left(D\frac{\partial^2 w}{\partial x^2}\right) + \rho A\frac{\partial^2 w}{\partial t^2} + q_2 = 0, \tag{2.17}$$

where

$$q_1 = be_{31}\frac{\partial V}{\partial x},$$

$$q_2 = be_{31}r_1\frac{\partial^2 V}{\partial x^2}.$$

Equations (2.16) and (2.17) are the governing equations representing the axial and transverse displacement of the sensor layer respectively.

3 Finite Element Formulation

The weak forms of the equations (2.16) and (2.17) over a typical element of length $\Delta^e = (0, l_e)$, of the discretized domain (the length of the sensor layer) are developed by first multiplying equation (2.16) and (2.17) by the weight functions $V_1(x)$ and $V_2(x)$ respectively and integrating over the element's length $\Delta^e = (0, l_e)$.
For equation (2.16):

$$\int_0^{l_e} V_1\left[-\frac{\partial}{\partial x}\left(G\frac{\partial u}{\partial x}\right) + \rho A\frac{\partial^2 u}{\partial t^2} + q_1\right]dx = 0, \tag{3.18}$$

$$\int_0^{l_e} V_1\left[-\frac{\partial}{\partial x}\left(G\frac{\partial u}{\partial x}\right)\right]dx + \int_0^{l_e} V_1\rho A\frac{\partial^2 u}{\partial t^2}dx + \int_0^{l_e} V_1 q_1 dx = 0. \tag{3.19}$$

Integrating the first term by parts and rearranging gives

$$\int_0^{l_e}\left[G\frac{\partial V_1}{\partial x}\frac{\partial u}{\partial x} + \rho A V_1\frac{\partial^2 u}{\partial t^2} + V_1 q_1\right]dx - V_1\left[G\frac{\partial u}{\partial x}\right]_0^{l_e} = 0. \tag{3.20}$$

IJMAO

International Journal of Mathematical Analysis and Optimization: Theory and Applications
Vol. 2020, No. 1, pp. 764 - 779

The coefficient of the weight function in the boundary terms are the secondary variables and are specified as the natural boundary conditions. That is

$$\int_0^{l_e} \left[G\frac{\partial V_1}{\partial x}\frac{\partial u}{\partial x} + \rho A V_1 \frac{\partial^2 u}{\partial t^2} + V_1 q_1 \right] dx - V_1(l_e)S_2^e - V_1(0)S_1^e = 0, \tag{3.21}$$

For equation (2.17):

$$\int_0^{l_e} V_2 \left[\frac{\partial^2}{\partial x^2}\left(D\frac{\partial^2 w}{\partial x^2} \right) + \rho A \frac{\partial^2 w}{\partial t^2} + q_2 \right] dx = 0, \tag{3.22}$$

$$\int_0^{l_e} V_2 \left[\frac{\partial^2}{\partial x^2}\left(D\frac{\partial^2 w}{\partial x^2} \right) \right] dx + \int_0^{l_e} V_2 \rho A \frac{\partial^2 w}{\partial t^2} dx + \int_0^{l_e} V_2 q_2 dx = 0. \tag{3.23}$$

Integrating the first term by part twice and rearranging all terms, give

$$\int_0^{l_e} \left[D\frac{\partial^2 V_2}{\partial x^2}\frac{\partial^2 w}{\partial x^2} + V_2 \rho A \frac{\partial^2 w}{\partial t^2} + V_2 q_2 \right] dx + \left[V_2 \frac{\partial}{\partial x}\left(D\frac{\partial^2 w}{\partial x^2} \right) - \frac{\partial V_2}{\partial x}\left(D\frac{\partial^2 w}{\partial x^2} \right) \right]_0^{l_e} = 0. \tag{3.24}$$

The boundary term consists of two essential boundary conditions and two natural boundary conditions. That is

$$\int_0^{l_e} \left[D\frac{\partial^2 V_2}{\partial x^2}\frac{\partial^2 w}{\partial x^2} + V_2 \rho A \frac{\partial^2 w}{\partial t^2} + V_2 q_2 \right] dx$$
$$- V_2(l_e)Q_3^e + \frac{\partial V_2(l_e)}{\partial x}Q_4^e - V_2(0)Q_1^e + \frac{\partial V_2(0)}{\partial x}Q_2^e = 0. \tag{3.25}$$

In equations (3.21) and (3.25),$V_1(x)$ and $V_2(x)$ are the weight functions; S_i^e $(i = 1, 2)$ as defined in equation (3.26), are the compressive and tensile forces at the boundaries; and Q_i^e $(i = 1, 2, 3, 4)$ as defined in equations (3.27) to (3.30), are the shear forces and bending moments at the boundaries.

$$S_1^e = -G\frac{\partial u}{\partial x}\bigg|_{x=0}; S_2^e = G\frac{\partial u}{\partial x}\bigg|_{x=l_e}, \tag{3.26}$$

$$Q_1^e = \frac{\partial}{\partial x}\left(D\frac{\partial^2 w}{\partial x^2} \right)\bigg|_{x=0} = -V(x_0), \tag{3.27}$$

$$Q_2^e = \left(D\frac{\partial^2 w}{\partial x^2} \right)\bigg|_{x=0} = -M(x_0), \tag{3.28}$$

$$Q_3^e = -\frac{\partial}{\partial x}\left(D\frac{\partial^2 w}{\partial x^2} \right)\bigg|_{x=l_e} = V(l_e), \tag{3.29}$$

$$Q_4^e = -\left(D\frac{\partial^2 w}{\partial x^2} \right)\bigg|_{x=l_e} = M(l_e). \tag{3.30}$$

Now, employing the Ritz technique, the weight function $V_1(x)$ is defined for the approximation function $\Phi(x)$ obtained from equation (3.21) using the Lagrange interpolation; and $V_2(x)$ is defined for the approximation function $\Psi(x)$ obtained from equation (3.25) using the Hermite cubic interpolation. These are respectively:

$$u(x,t) = \sum_{j=1}^{2} \phi_j(x)u_j(t), \tag{3.31}$$

$$w(x,t) = \sum_{j=1}^{4} \psi_j(x)w_j(t), \tag{3.32}$$

IJMAO

International Journal of Mathematical Analysis and Optimization: Theory and Applications
Vol. 2020, No. 1, pp. 764 - 779

where

$$\Phi_1(x) = \left(1 - \frac{x}{l_e}\right); \Phi_2(x) = \left(\frac{x}{l_e}\right); \tag{3.33}$$

$$\Psi_1(x) = 1 - 3\left(\frac{x}{l}\right)^2 + 2\left(\frac{x}{l}\right)^3; \quad \Psi_2(x) = -x\left(1 - \frac{x}{l}\right)^2;$$

$$\Psi_3(x) = 3\left(\frac{x}{l}\right)^2 - 2\left(\frac{x}{l}\right)^3; \quad \Psi_4(x) = -x\left(\left(\frac{x}{l}\right)^2 - \frac{x}{l}\right). \tag{3.34}$$

Equation (3.31) in (3.21) and (3.32) in (3.25) yield the following set of equations of motion, respectively for the axial and transverse displacement, for a typical element

$$\sum_{j=1}^{2} k_{ij}u_j + \sum_{j=1}^{2} m_{ij}\ddot{u}_j = -F_i + Q_i, \tag{3.35}$$

$$\sum_{j=1}^{4} k^*_{ij}w_j + \sum_{j=1}^{4} m^*_{ij}\ddot{w}_j = -F^*_i + Q^*_i. \tag{3.36}$$

The terms in equations (3.35) and (3.36) are as defined in equations (3.37) and (3.38) respectively. They are the element stiffness matrices, element mass matrices, the element applied force and the element internal generalized forces.

$$k_{ij} = \int_0^{l_e} G\phi_i'\phi_j' dx; \quad m_{ij} = \int_0^{l_e} \rho A\phi_i\phi_j dx \quad and$$

$$F_i = \int_0^{l_e} \phi_i q_1 dx; \quad Q_i = \phi_i(l_e)Q_2^e - \phi_i(0)Q_1^e, \tag{3.37}$$

$$k^*_{ij} = \int_0^{l_e} D\psi_i''\psi_j'' dx; \quad m^*_{ij} = \int_0^{l_e} \rho A\psi_i\psi_j dx F^*_i = \int_0^{l_e} \psi_i q_2 dx \quad and$$

$$Q^*_i = \psi_i(0)Q_1^e + \psi_i(l_e)Q_3^e - \psi_i'(0)Q_2^e - \psi_i'(l_e)Q_4^e. \tag{3.38}$$

Evaluating equations (3.37) and (3.38) using (3.33) and (3.34) respectively, the matrices and applied forces in (3.37) and (3.38) becomes

$$k = \frac{G}{l_e}\begin{pmatrix} 1 & -1 \\ -1 & 1 \end{pmatrix}; \; m = \frac{\rho A l_e}{6}\begin{pmatrix} 2 & 1 \\ 1 & 2 \end{pmatrix}; \; F = \frac{q_1 l_e}{2}\begin{Bmatrix} 1 \\ 1 \end{Bmatrix}. \tag{3.39}$$

$$k^* = \frac{2D}{l_e^3}\begin{bmatrix} 6 & -3l_e & -6 & -3l_e \\ -3l_e & 2l_e^2 & 3l_e & l_e^2 \\ -6 & 3l_e & 6 & 3l_e \\ -3l_e & l_e^2 & 3l_e & 2l_e^2 \end{bmatrix}; \; m^* = \frac{\rho A l_e}{420}\begin{bmatrix} 156 & -22l_e & 54 & -13l_e \\ -22l_e & 4l_e^2 & 13l_e & -3l_e^2 \\ 54 & -13l_e & 156 & 22l_e \\ 13l_e & -3l_e^2 & 22l_e & 4l_e^2 \end{bmatrix};$$

$$F^* = \frac{q_2 l_e}{12}\begin{Bmatrix} 6 \\ -l_e \\ 6 \\ l_e \end{Bmatrix}. \tag{3.40}$$

IJMAO

International Journal of Mathematical Analysis and Optimization: Theory and Applications
Vol. 2020, No. 1, pp. 764 - 779

4 Finite Element Models

Following the standard procedure of the fiinite element method, Reddy [10], the elemental equations of motion (3.35) and (3.36) are assembled. The clamped boundary conditions of equations (4.41) and (4.42) are imposed respectively for the axial and transverse equations.

$$u(0,t) = u(L,t) = 0; \quad Q_1^1 = -Q_2^2 = -\left[a\frac{du}{dx}\right]; Q_2^1 + Q_1^2 = 0; \tag{4.41}$$

$$w(0,t) = \frac{dw(L,t)}{dx} = 0; \quad Q_3^1 + Q_1^2 = Q_4^1 + Q_2^2 = 0. \tag{4.42}$$

The finite element model for the axial loading is obtained by substituting the approximation function (3.31) into the weak form (3.21). That is

$$\int_0^{l_e}\left[G\frac{d\phi_i}{dx}\frac{d}{dx}\left(\sum_{j=1}^{2}\phi_j u_j\right) + \rho A\phi_i\frac{d^2}{dt^2}\left(\sum_{j=1}^{2}\phi_j u_j\right) + \phi_i q_1\right]dx - \phi_i(l_e)Q_2^e - \phi_i(0)Q_1^e = 0, \tag{4.43}$$

that is

$$\sum_{j=1}^{2}\left[\int_0^{l_e}\left(G\frac{d\phi_i}{dx}\frac{d\phi_j}{dx}u_j + \rho A\phi_i\phi_j\frac{d^2u_j}{dt^2}\right)dx\right] + \int_0^{l_e}\phi_i q_1 dx - \phi_i(l_e)Q_2^e - \phi_i(0)Q_1^e = 0, \tag{4.44}$$

this yieds

$$\sum_{j=1}^{2}[K_{ij}u_j + M_{ij}\ddot{u}_j - Q_i] + F_i = 0. \tag{4.45}$$

Where

$$K_{ij} = \int_0^{l_e} G\frac{d\phi_i}{dx}\frac{d\phi_j}{dx}dx, \quad M_{ij} = \int_0^{l_e}\rho A\phi_i\phi_j dx, \quad Q_i = \sum_{i=1}^{2}\phi_i(x_i)Q_i^e, \quad F_i = \int_0^{l_e}\phi_i q_1 dx \tag{4.46}$$

The finite element model for the transverse loading is similarly obtained by substituting the approximation function (3.32) into the weak form (3.25). That is

$$\int_0^{l_e}\left[D\frac{d^2\psi_i}{dx^2}\frac{d^2}{dx^2}\left(\sum_{j=1}^{4}\psi_j w_j\right) + \psi_i\rho A\frac{d^2}{dt^2}\left(\sum_{j=1}^{4}\psi_j w_j\right) + \psi_i q_2\right]dx$$

$$- \psi_i(0)Q_1^e + \frac{d\psi_i(0)}{dx}Q_2^e - \psi_i(l_e)Q_3^e + \frac{d\psi_i(l_e)}{dx}Q_4^e = 0, \tag{4.47}$$

$$\sum_{j=1}^{4}\int_0^{l_e}\left(D\frac{d^2\psi_i}{dx^2}\frac{d^2}{dx^2}w_j + \rho A\psi_i\psi_j\frac{d^2w_j}{dt^2}\right)dx + \int_0^{l_e}\psi_i q_2 dx$$

$$- \psi_i(0)Q_1^e - \psi_i(l_e)Q_3^e + \frac{d\psi_i(0)}{dx}Q_2^e + \frac{d\psi_i(l_e)}{dx}Q_4^e = 0, \tag{4.48}$$

$$\sum_{j=1}^{4}\left[\int_0^{l_e}\left(D\frac{d^2\psi_i}{dx^2}\frac{d^2\psi_j}{dx^2}w_j\right)dx + \int_0^{l_e}\rho A\psi_i\psi_j\frac{d^2w_j}{dt^2}dx + \int_0^{l_e}\psi_i q_2 dx - Q_i^e\right] = 0. \tag{4.49}$$

This yields

$$\sum_{j=1}^{4}[K_{ij}w_j + M_{ij}\ddot{w}_j] = \sum_{i=1}^{4}[-F_i + Q_i^e] \tag{4.50}$$

IJMAO

International Journal of Mathematical Analysis and Optimization: Theory and Applications
Vol. 2020, No. 1, pp. 764 - 779

Where

$$K_{ij} = \int_0^{l_e} \left(D \frac{d^2\psi_i}{dx^2} \frac{d^2\psi_j}{dx^2} \right) dx, \quad M_{ij} = \int_0^{l_e} \rho A \psi_i \psi_j dx, \quad F_i = \int_0^{l_e} \psi_i q_2 dx$$

$$Q_i = \psi_i(0) Q_1^e + \psi_i(l_e) Q_3^e - \frac{d\psi_i(0)}{dx} Q_2^e - \frac{d\psi_i(l_e)}{dx} Q_4^e, \tag{4.51}$$

The resulting finite element model for the axial loading from equation (4.45) is a system of three equations in three unknowns, while the model for the transverse loading from (4.50) is a system of six equations in six unknowns. They are both given as equations (4.52) and (4.53) respectively.

$$KU + M\ddot{U} = L, \tag{4.52}$$

$$K^*W + M^*\ddot{W} = L^*. \tag{4.53}$$

where K and M are the structural stiffness and mass matrices respectively; U and $\ddot{U}$ are vectors of the axial structural displacement and acceleration respectively; W and $\ddot{W}$ are vectors of the transverse structural displacement and acceleration respectively; L (L^*) is the addition of the assembled applied forces vector F (F^*) and the assembled internal generalized forces vector Q (Q^*).
The Newmark method was used to fully discretize the semidiscrete second order time derivatives in (52) and (53), after first rewriting them in two time steps, and subtracting the previous time from the current time, as follows:

$$K\Delta u_i + M\Delta\ddot{u}_i = \Delta L_i, \tag{4.54}$$

$$K^*\Delta w_i + M^*\Delta\ddot{w}_i = \Delta L_i^*. \tag{4.55}$$

Newmark's method with the linear acceleration option ($\beta = \frac{1}{6}$) transforms of equations (4.54) and (4.55) to:

$$\hat{K}\Delta u_i = \Delta\hat{L}_i, \tag{4.56}$$

$$\hat{K}^*\Delta w_i = \Delta\hat{L}_i^*, \tag{4.57}$$

where

$$\hat{K} = \left(K + M\frac{1}{\beta\Delta t^2} \right), \quad \Delta\hat{L}_i = \Delta L_i + M\frac{1}{\beta\Delta t}\dot{u}_i + M\frac{1}{2\beta}\ddot{u}_i, \tag{4.58}$$

$$\hat{K}^* = \left(K^* + M^*\frac{1}{\beta\Delta t^2} \right), \quad \Delta\hat{L}_i^* = \Delta L_i^* + M^*\frac{1}{\beta\Delta t}\dot{w}_i + M^*\frac{1}{2\beta}\ddot{w}_i. \tag{4.59}$$

In equations (4.58) and (4.59), β defines the variation of acceleration over a time step and determines stability and accuracy, typically $\frac{1}{6} \leq \beta \leq \frac{1}{4}$, $\Delta t = t_{i+1} - t_i$. According to Chopra [11], the stability requirement for the Newmark method is

$$\frac{\Delta t}{T_n} \leq \frac{1}{\pi\sqrt{2}} \frac{1}{\sqrt{0.5 - 2\beta}}, \tag{4.60}$$

where T_n is the natural period of vibration. For this study, the method is stable if

$$\frac{\Delta t}{T_n} \leq 0.551. \tag{4.61}$$

This was achieved with $\Delta t = 0.1$. Shorter time steps than $0.551T_n$ gives more accurate representation of the excitations and responses.

IJMAO

International Journal of Mathematical Analysis and Optimization: Theory and Applications
Vol. 2020, No. 1, pp. 764 - 779

5 Numerical Investigation and Result

Using the fully discrete finite element models of (56) and (57), the responses of the piezoelectric sensor layer of the beam is considered. The host beam is made of a $[0^0, 90^0]$ composite material. The average thickness of the beam is 1.94mm, and the ply thickness is 0.161mm. The beam is clamped at its left end and its effective length is 30cm. A 10.3cm long and 0.0762mm thick piezoelectric sensor is bonded on the upper surface of the composite beam and its left ends are 3.4cm away from the clamped end of the host beam. The mass density of the beam and the piezoelectric actuator are $1507kgm^{-3}$ and $5000kgm^{-3}$ respectively. The Young's modulus of the piezoelectric sensor is 6.9GPa. The equivalent bending stiffness and extension stiffness for the composite beam with unit width are calculated as $D = 45.5196Nm^2$ and $G = 1.19795 \times 10^{10}N$. In our calculation, the thickness of the adhesive layer is taken as 0.1mm. The axial displacement is obtained using the parameter values: $\rho = 1000$, $G = 1.19795 \times 10^{10}$, $l_e = 0.2$, and $q_1 = 100$. These parameter values were also used in the study of Sun et al. (2001) [8].
From fig. 3, by increasing the values of G we observed that the axial displacement values increased as time increased. Similar trends were observed by raising the values of A on axial displacement as can be seen from fig. 4, and fig. 5 - by increasing the density ρ values in fig. 5.

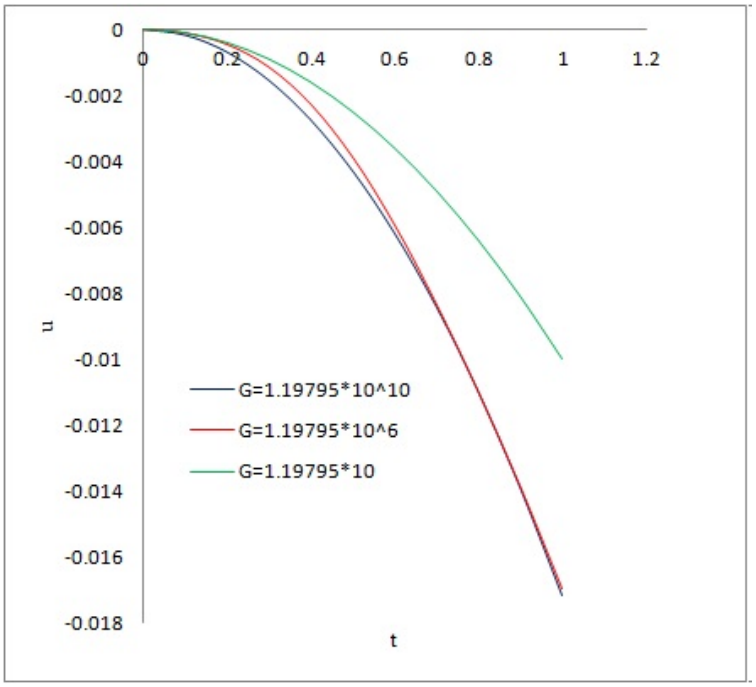

Figure 3: Effect of Extension Stiffness (G) on the Axial Displacement.

IJMAO

International Journal of Mathematical Analysis and Optimization: Theory and Applications
Vol. 2020, No. 1, pp. 764 - 779

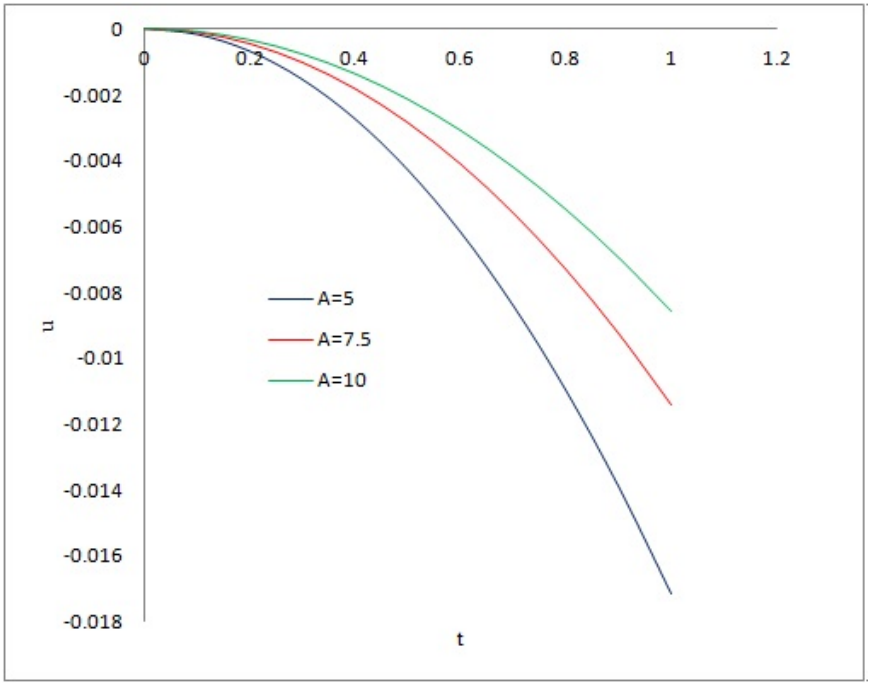

Figure 4: Effect of Area (A) on the Axial Displacement.

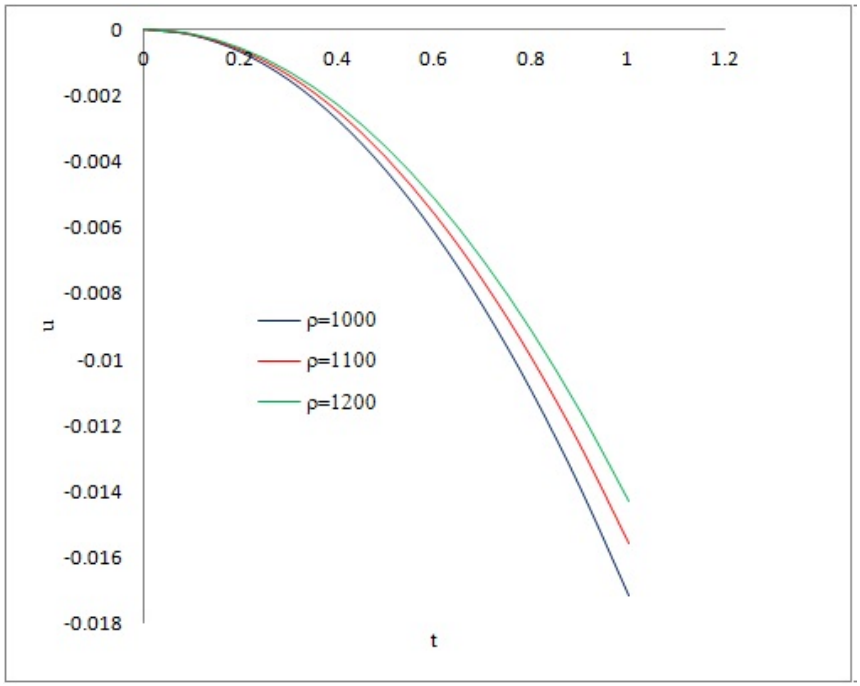

Figure 5: Effect of Pressure (ρ) on the Axial Displacement.

IJMAO

International Journal of Mathematical Analysis and Optimization: Theory and Applications
Vol. 2020, No. 1, pp. 764 - 779

	dverk78 - 7th-8th order continuous Runge-Kutta method **ck45** - Cash-Karp fourth-fifth order Runge-Kutta method **taylorseries** - Taylor series method.			Linear Acceleration option. $\beta = \frac{1}{6}$
t	taylorseries	ck45	dverk78	Newmark-β
0	0	0	0	0
0.1	-0.000171399	-0.000171398	-0.000171399	-0.000171399
0.2	-0.000685669	-0.000685667	-0.000685669	-0.000685666
0.3	-0.00154285	-0.001542852	-0.00154285	-0.001542849
0.4	-0.002742846	-0.002742849	-0.002742846	-0.002742853
0.5	-0.004285668	-0.004285661	-0.004285668	-0.004285664
0.6	-0.006171403	-0.006171402	-0.006171403	-0.006171395
0.7	-0.0084	-0.008400009	-0.0084	-0.008400009
0.8	-0.010971394	-0.01097139	-0.010971394	-0.010971401
0.9	-0.013885672	-0.013885661	-0.013885672	-0.013885656
1	-0.017142853	-0.017142864	-0.017142853	-0.017142852

Table 1: Computations showing the comparison of Newmark with some numerical methods for the Axial Displacement, U.

For all cases, by increasing the specified physical parameter values, the axial displacement of the debonded piezoelectric actuator layer increased with respect to time.
The parameter values for the composite beam used to obtain the transverse displacement according to [8] are: $\rho = 1000$, $D = 49.5196$, $l_e = 0.5$, $A = 5$ and $q_2 = 100$.
Following a similar approach, by varying(increasing) the Axial stiffness D, as can be seen in fig. 6, the transverse displacement of the debonded piezoelectric sensor layer tends to increase, and then losses control after time $t = 0.3s$). The same is observed from fig. 7, by increasing the Area A, and fig. 8, by increasing the Density ρ. In both fig. 7 and fig. 8, the transverse vibration of the debonded piezoelectric sensor layer also losse control and becomes boundless.
The effects of these parameters on the transverse displacement of the debonded piezoelectric sensor layer, as shown in figs. 6, 7, and 8, are indications that the actuator layer loses contact with the host beam due to increase in the debonding length caused by the increases of the Bending stiffness, Area, and Density of the composite beam respectively.

IJMAO

International Journal of Mathematical Analysis and Optimization: Theory and Applications
Vol. 2020, No. 1, pp. 764 - 779

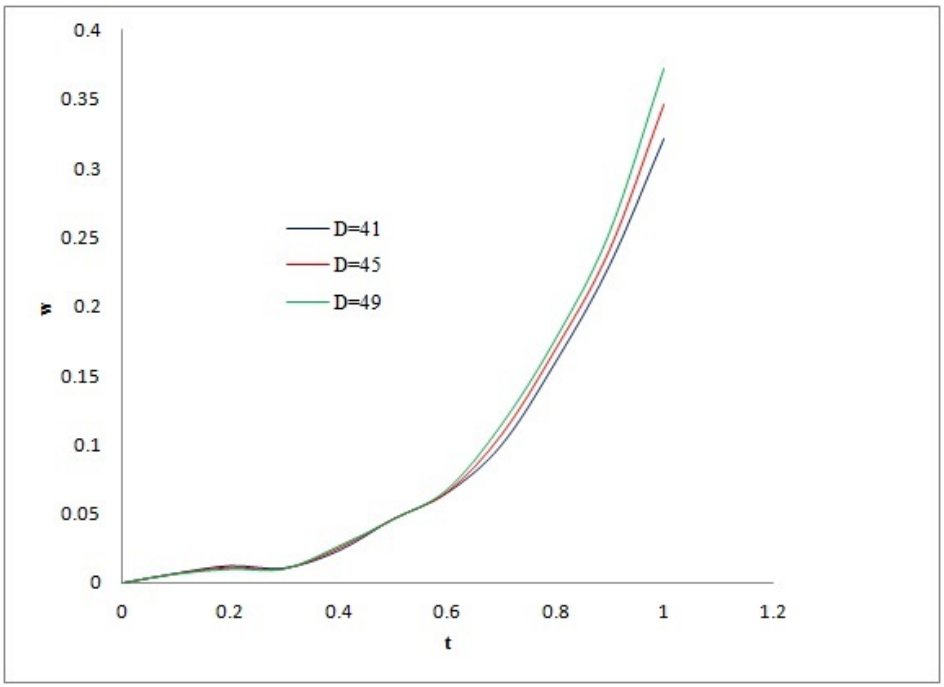

Figure 6: Effect of Bending Stiffness (D) on the Transverse Displacement.

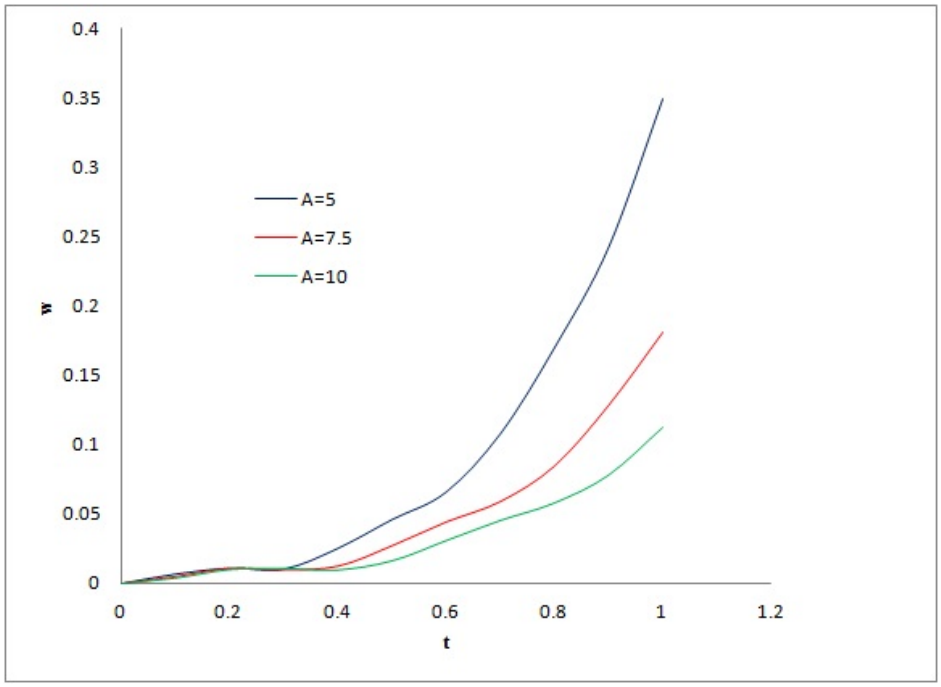

Figure 7: Effect of Area (A) on the Transverse Displacement.

IJMAO

International Journal of Mathematical Analysis and Optimization: Theory and Applications
Vol. 2020, No. 1, pp. 764 - 779

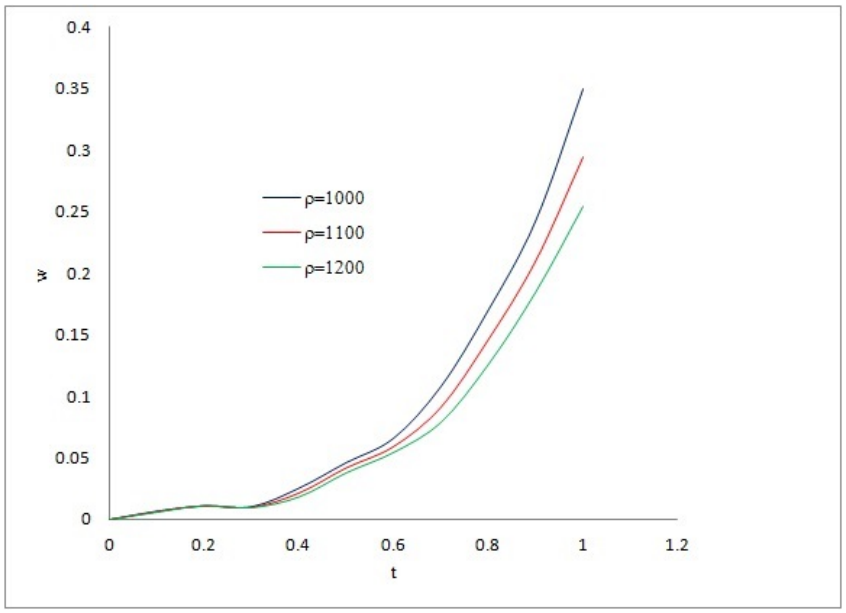

Figure 8: Effect of Pressure (ρ) on the Transverse Displacement.

6 Concluding Remarks

A dynamic analysis has been carried out to study the effects of some physical parameters on a debonding piezoelectric using the finite element method. The results obtained in the study reveal the following:

1. An increase in axial stiffness of the composite beam increases the axial displacement of the debonding piezoelectric actuator layer.
2. An increase in area of the composite beam enhances the axial displacement of the debonding piezoelectric actuator layer.
3. The axial displacement of the piezoelectric actuator layer also increase as a result of an increment in the composite beam's density.
4. Increasing the value of the bending stiffness of the composite beam decreases the transverse displacement of the debonding piezoelectric actuator layer. With a boundless swing noticed from $t = 0.3s$.
5. An increase in the area of the composite beam also decreases the transverse displacement of the debonding piezoelectric actuator layer. A boundless swing was observed after $t = 0.3s$ for $A = 5$, $t = 0.4s$ for $A = 10$, and at $t = 0.6s$ for $A = 20$.
6. An increment in the density of the composite beam results in a decrease in the transverse displacement of the piezoelectric actuator layer. And a boundless swing was observed after $t = 0.3s$ for $\rho = 1000$, $t = 0.4s$ for $\rho = 1500$, and at $t = 0.5s$ for $\rho = 3000$.

The impact of the variations of the specified physical parameters, especially on the transverse displacement, has far reaching implications on the debonding of the piezoelectric actuator layer in the composite beam. As seen in figs. 6, 7, and 8, the displacements become boundless after some time. This situation will worsen the control of the host beam because it will result in there being no contact between the host beam and the piezoelectric patches. This will negatively impact on the control function of the smart structure.

	dverk78 - 7th-8th order continuous Runge-Kutta method **ck45** - Cash-Karp fourth-fifth order Runge-Kutta method **taylorseries** - Taylor series method.			Linear Acceleration option. $\beta = \frac{1}{6}$
t	taylorseries	ck45	dverk78	Newmark-β
0	0	0	0	0
0.1	0.006829388	0.006829388	0.006829388	0.006829389
0.2	0.011086314	0.011086316	0.011086314	0.011086317
0.3	0.010422745	0.010422742	0.010422745	0.010422739
0.4	0.025470327	0.025470323	0.025470327	0.025470327
0.5	0.04621225	0.046212255	0.04621225	0.046212261
0.6	0.066052266	0.066052266	0.066052266	0.066052254
0.7	0.108126094	0.108126092	0.108126094	0.108126086
0.8	0.17017469	0.170174701	0.17017469	0.170174712
0.9	0.242670405	0.242670409	0.242670405	0.242670393
1	0.349514928	0.34951492	0.349514928	0.349514906

Table 2: Computations showing the comparison of Newmark with some numerical methods for the Tranverse Displacement, W.

Competing Financial Interests

The authors declare no competing financial interests.

References

[1] Kerboua, M., Megnounif, A., Benguediab, M., Benrahou, K.H., Kaoulala, M.F. Vibration Control Beam Using Piezoelectric-Based Smart Materials. *Composite Structures*, vol. 123, issue 5, pp. 430-442 (2015),
DOI: 10.1016/j.compstruct.2014.12.044

[2] Gandhi, P.K., Mevada, J.R. A Finite Element Model and Active Vibration Control of Composite Beams With Distributed Piezoelectric Using Third Order Theory. *IJERA*, vol. 3, issue 3, pp. 940-945, (2013).

[3] Sohrabi,M.A., Muliana, A. H. Nonlinear and Time Dependent behaviours of Piezoelectric Materials and Structures. *International. Journal of Mechanical Sciences. Elsevier*, vol. 166, pp. 26-45, (2015).

[4] Lezgy-Nazargah M., Vidal P., Polit O. An Efficient Finite Element Model for Static and Dynamic Analyses of Functionally Graded Piezoelectric Beams. *Composite Structures*, vol. 104, pp. 71-84, (2013).

[5] Seely, C. E., Chattopadhyay A. ExperimentalInvestigation of Composite Beams with Piezoelectric Actuation and Debonding Smart Material. *International Journal of Solids and Structures*, vol. 7, pp. 502-511, (1998).

[6] Shijie, Z. Finite Element Analysis of Smart Structures with Piezoelectric Sensors/Actuators Including Debonding. *Chinese Journal of Aeronautics*, vol 17, pp. 246-250, (2004).

[7] Neto, M. A., Yu, W., Roy, S. Two Finite Elements for General Composite Beams with Piezoelectric Actuators and Sensors. *Finite Elements in Analysis and Design*, vol. 45, pp. 295-304, (2009).

[8] Sun D.C., Tong L., Atluri S.N. Effects of Piezoelectric Sensor/Actuator Debonding on Vibration Control of Smart Beams. . *J. Solids Struct.* vol. 38, issue 18, pp. 9033-9051, (2001).

[9] Alaimo, A., Milazzo, A., Orlando, C., Messineo, A. Numerical Analysis of Piezoelectric Active Repair in the Presence of Frictional Contact Conditions. *Sensors* , vol. 13, issue 4, pp. 4390-4403, (2013).
https://doi.org/10.3390/s130404390.

[10] Reddy, J.N. An Introduction to the Finite Element Method (3ed). McGraw-Hill International Edition, New York. (2006).

[11] Chopra, A.K. Dynamics of Structures: Theory and Applications to Earthquake Engineering (5ed). Pearson Education Limited, Harlow UK. (2020).